SEMARAK ILMU PUBLISHING

CFD Letters

Journal homepage:
https://semarakilmu.com.my/journals/index.php/CFD_Letters/index
ISSN: 2180-1363

Numerical Simulation of Pipeline Scour and Sedimentation around Submerged Pipelines with an Open-Source Multiphase-CFD Model

Subiyanto[1,2,*], Novan Tofany[2]

[1] Department of Marine Science, Faculty of Fishery and Marine Science, Universitas Padjadjaran, Sumedang 45363, Indonesia
[2] Research Center for Computing, National Research and Innovation Agency (BRIN), Soekarno Science and Technology Zone, Cibinong 16911, Indonesia

ARTICLE INFO

Article history:
Received 9 October 2023
Received in revised form 12 November 2023
Accepted 15 December 2023
Available online 29 February 2024

Keywords:
Pipelines; Scouring; Sedimentation; Multiphase-Model, CFD

ABSTRACT

This paper presents a comprehensive study on pipeline scour and sedimentation phenomena using an open-source multiphase Computational Fluid Dynamics (CFD) model. The research focuses on understanding the complex interactions between fluid flow, sediment transport, and scour formation around submerged pipelines. The proposed analysis aims to enhance the understanding of scour development and sedimentation deposition, which is crucial for the design, operation, and maintenance of various engineering structures, including offshore pipelines and underwater infrastructure. The results show that the model exhibits the ability to compute sediment transport without depending on traditional assumptions related to bed-load and suspended-load layers. The simulation results affirm the model's proficiency in replicating the underlying mechanisms accountable for the onset of these processes, notably seepage flow and piping. Furthermore, this model can successfully depict the vortex phenomenon, which promotes the accumulation of sediment around the pipe. This phenomenon arises from the contrast in pressure between the centre of the vortex and the pressure exerted on the sediment beneath it.

1. Introduction

Pipelines play a vital role in transporting various fluids, such as water, oil, and gas, across vast distances, both onshore and offshore [1]. However, their successful operation and long-term integrity depend on the dynamic interactions between the flowing fluid and the surrounding sediment in marine environments. The scouring of sediment and sedimentation around submerged pipelines are two critical phenomena that can significantly impact pipeline performance and safety [2]. Understanding these complex processes is of paramount importance for the design, operation, and maintenance of underwater infrastructures [3, 4].

Scour, the process of sediment erosion around submerged structures, is a natural consequence of fluid flow and can lead to undesirable consequences, such as pipeline exposure, reduced stability, and potential structural damage [5, 6]. Around a pipeline resting on the seabed and exposed to waves

* *Corresponding author.*
E-mail address: subiyanto@unpad.ac.id, subi008@brin.go.id (Subiyanto)

https://doi.org/10.37934/cfdl.16.7.150165

and/or currents, various local flow alterations occur, including flow constriction, vortices, seepage flow, and turbulence [7, 8]. These flow phenomena result in localized sediment transport and subsequently the creation of scour trenches, which progress through three successive phases: the initiation of scour, tunnel erosion, and lee-wake erosion [7, 9, 10].

The initiation of scour is initiated by a pressure difference between the upstream and downstream sides, leading to seepage flow beneath the pipeline. Following this, a small gap forms beneath the pipeline through a process known as piping [8], allowing the incoming flow to enter and enabling tunnel erosion. The primary expansion of the trench predominantly takes place during the tunnel erosion stage, during which sediments are swiftly transported over a brief period [11]. This is driven by the creation of high-velocity jet-like flows beneath the pipe, resulting in high bed shear stresses. As the trench expands, free-span regions may emerge, causing increased stress and structural fatigue. On the other hand, sedimentation, the deposition of transported sediment particles in the vicinity of the pipe. Sedimentation has the potential to enhance the stability of the pipeline on the seabed by reducing the hydrodynamic drag on the pipeline and increasing the lateral soil resistance [12]. Furthermore, alterations in the lateral soil resistance (and to a lesser degree, axial resistance) can also impact the design considerations for thermal expansion [13]. The added insulation provided by the surrounding soil can modify the temperature distribution along the pipeline, with potential consequences for various aspects of flow assurance, including the management of top-of-line corrosion. Accurate prediction and assessment of scour and sedimentation phenomena are, therefore, essential for ensuring the optimal functioning and longevity of underwater pipelines [14].

Over the years, experimental studies [7-9, 15-19] and numerical simulations [20-27] have been employed to investigate pipeline scour and sedimentation. Nonetheless, classical single models have certain shortcomings that restrict their suitability for ad-dressing intricate interactions between fluids, sediment, and pipelines. For example, several pipeline scour modelling studies [23, 28] showed that these models suffer numerical instability when there is a direct contact between the pipe and the seabed, which is crucial in simulating the onset of scour and partial-buried pipeline sedimentation. To address these challenges and improve the accuracy of pipeline scour and sedimentation analysis, this paper introduces a novel approach utilizing an open-source multiphase Computational Fluid Dynamics (CFD) model named OpenFOAM. Several researchers also utilize OpenFoam in their study [29-31]. The use of a multiphase CFD model allows us to simulate the simultaneous interactions of the fluid and sediment phases, providing a more comprehensive understanding of scour and sedimentation processes. Furthermore, the open-source nature of the model ensures transparency, flexibility, and accessibility for researchers and engineers, promoting collaboration and advancing the state-of-the-art in this field.

The primary objective of this research is to exhibit the phenomena that occur into pipeline scour and sedimentation using the open-source multiphase CFD model. This study aims to shed light on the complex interactions between fluid dynamics, sediment transport, and pipe in the context of scour and sedimentation process. The findings of this research will have practical implications for engineering design, pipeline integrity management, and environmental protection, enabling the development of effective strategies to mitigate scour and sedimentation risks. In the subsequent sections of this paper, a comprehensive analysis of pipeline scour and sedimentation under varying conditions. This research seeks to contribute to the scientific understanding and engineering practices related to pipeline scour and sedimentation in marine environments.

2. Model Description

The model applied in this study builds upon Lee's multiphase model [32], which is based on the Navier-Stokes equations for both the fluid and sediment phases [32].The model is briefly introduced in this section, while the model formulas is summarized in Table 1 and parameters is provided in Table 2. The detailed descriptions of the model can be referred to Lee *et al.,* [32]. Developing in an open-source CFD platform named OpenFOAM, the model assumes both the sediment and fluid (water) phases as incompressible medium, which share a space with volume phase fractions ϕ_1 and ϕ_2, respectively. The governing equations consist of two sets of mass and momentum balance equations, one for each phase. Each set of equations involves the phase fraction ϕ_i and velocity vector $\mathbf{u}_i$, where the subscript can represent either the sediment (1) or fluid (2) phase. To represent sediment kinematics and seabed mobility, the model considers the rheological characteristics of sediment particles in both static and mobile states, as well as the influence of fluid on these interactions. Turbulence in the flow is computed using the two-phase $k-\varepsilon$ model, which also accounts for the impact of sediment in dampening turbulence. The exchange of momentum between the fluid and sediment phases is captured through drag force and turbulent dispersion. The computation of particle stresses and pressure is achieved through constitutive models, considering the rheological properties of the fluid-sediment mixture, the elastic behavior of sediment particles in a static state, and the influence of fluid turbulence and sediment turbulent motions. In this study, an enhancement involves the incorporation of additional body force terms in the momentum equations, which were not included in the original model.

Table 1
Model formulation

Mass balance and momentum balance equations of the sediment phase:
$\frac{\partial \rho_1 \phi_1}{\partial t} + \nabla \cdot \left[\rho_1 \phi_1 \mathbf{u}_1 \right] = 0$
$\frac{\partial \rho_1 \phi_1 \mathbf{u}_1}{\partial t} + \nabla \cdot \left[\rho_1 \phi_1 \mathbf{u}_1 \mathbf{u}_1 \right] = -\rho_1 \phi_1 \mathbf{g} - \phi_1 \nabla p_2 - \nabla \left(\phi_1 p_1 \right) + \nabla \cdot \left[\phi_1 \mathbf{T}_1 \right] + \left\{ \phi_1 \rho_1 \frac{\mathbf{u}_2 - \mathbf{u}_1}{\tau_p} - \frac{\rho_1}{\tau_p} \frac{\phi_2 \nu_{2t}}{\sigma_c} \nabla \phi_1 \right\} + \phi_1 \mathbf{F}_b$
Mass balance and momentum balance equations of the fluid phase:
$\frac{\partial \rho_2 \phi_2}{\partial t} + \nabla \cdot \left[\rho_2 \phi_2 \mathbf{u}_2 \right] = 0$
$\frac{\partial \rho_2 \phi_2 \mathbf{u}_2}{\partial t} + \nabla \cdot \left[\rho_2 \phi_2 \mathbf{u}_2 \mathbf{u}_2 \right] = -\rho_2 \phi_2 \mathbf{g} - \phi_2 \nabla p_2 + \nabla \cdot \left[\phi_2 \mathbf{T}_2 \right] - \left\{ \phi_2 \rho_2 \frac{\mathbf{u}_2 - \mathbf{u}_1}{\tau_p} - \frac{\rho_1}{\tau_p} \frac{\phi_2 \nu_{2t}}{\sigma_c} \nabla \phi_1 \right\} + \phi_2 \mathbf{F}_b$
Body force:
$\mathbf{F}_b = 0$, **for scour simulation**
$\mathbf{F}_b = \left(F_x, 0, 0 \right)$, **where** $\mathbf{F}_x = \rho_2 \frac{\partial}{\partial t} \left[u_m \sin \left(\frac{2\pi t}{T} \right) \right]$, **for sedimentation simulation**
The gravitational acceleration is $\mathbf{g} = \left(0, -9.81, 0 \right)\ \mathrm{m/s^2}$
Governing equations of the two-phase $k-\varepsilon$ **turbulence model:**

$$\frac{\partial \rho_2 \phi_2 k}{\partial t} + \nabla \cdot \left[\rho_2 \phi_2 \mathbf{u}_2 k \right] = \phi_2 \mathbf{T}_2 : \nabla \mathbf{u}_2 - \rho_2 \phi_2 \varepsilon + \nabla \cdot \left[\rho_2 \frac{\nu_{2t}}{\sigma_k} \phi_2 k \right] - \left\{ \left(\rho_1 - \rho_2 \right) \frac{\phi_2 \nu_{2t}}{\sigma_c} \nabla \phi_1 \cdot \mathbf{g} + \frac{2 \rho_2 \phi_2 \left(1 - \alpha \right) k}{\tau_p} \right\}$$

$$\frac{\partial \rho_2 \phi_2 \varepsilon}{\partial t} + \nabla \cdot \left[\rho_2 \phi_2 \mathbf{u}_2 \varepsilon \right] = \frac{\varepsilon}{k} \left[C_{\varepsilon 1} \phi_2 \mathbf{T}_2 : \nabla \mathbf{u}_2 - C_{\varepsilon 2} \rho_2 \phi_2 \varepsilon \right] - \rho_2 \phi_2 \varepsilon + \nabla \cdot \left[\rho_2 \frac{\nu_{2t}}{\sigma_\varepsilon} \phi_2 \varepsilon \right] - \frac{\varepsilon}{k} C_{\varepsilon 3} \left\{ \left(\rho_1 - \rho_2 \right) \frac{\phi_2 \nu_{2t}}{\sigma_c} \nabla \phi_1 \cdot \mathbf{g} + \frac{2 \rho_2 \phi_2 \left(1 - \alpha \right) k}{\tau_p} \right\}$$

where the eddy viscosity is

$$\nu_{2t} = \frac{C_\mu k^2}{\varepsilon}$$

and

$$\alpha = \left(1 + \frac{\tau_p}{\min \left(0.165 \frac{k}{\phi_1}, \left[\left(\frac{\phi_{1rcp}}{\phi_1} \right)^{1/3} - 1 \right] \left(\frac{\rho_1}{p_1} \right)^{1/2} \right)} \right)^{-1}$$

Fluid stress tensor:

$$\mathbf{T}_2 = \rho_2 \left(\nu_{2t} + \nu_2 \right) \left[\nabla \mathbf{u}_2 + \left(\nabla \mathbf{u}_2 \right)^T \right] - \frac{2}{3} \rho_2 \left(k + \nu_{2t} \nabla \cdot \mathbf{u}_2 \right) \mathbf{I}$$

where $\mathbf{I}$ is the identity matrix

Sediment pressure [35]:

$$p_1 = p_{1r} + p_{1e} + p_{1t}$$

where

$$p_{1r} = \frac{2 b^2 \phi_1}{\left(\phi_{1c} - \phi_1 \right)} \left(\rho_2 \nu_{2t} + 2 a \rho_1 d^2 D_1 \right) D_1, \text{ with } D_1 = \frac{\left[\nabla \mu_1 + \left(\nabla \mu_1 \right)^T \right]}{2}$$

$$p_{1e} = K \left[\left(\phi_1 - \phi_{1o}, 0 \right) \right]^{1.5} \left\{ 1 + \sin \left[\left(\frac{\phi_1 - \phi_{1o}}{\phi_{1rcp} - \phi_{1o}}, 0 \right) \pi - \frac{\pi}{2} \right] \right\}$$

$$p_{1t} = \frac{2}{3} \rho_1 \alpha k$$

Sediment stress [35]:

$$\mathbf{T}_1 = \rho_1 \nu_1 \left[\nabla \mathbf{u}_1 + \left(\nabla \mathbf{u}_1 \right)^T \right] - \frac{2}{3} \rho_1 \nu_1 \nabla \cdot \mathbf{u}_1 \mathbf{I}$$

where the sediment kinematic viscosity is defined as

$$\nu_1 = \nu_{1\upsilon} + \nu_{1t}$$

with

$$\nu_{1\upsilon} = \frac{\left(p_{1r} + p_{1e} \right) \eta}{2 \rho_1 D_1}, \text{ and}$$

$$\nu_{1t} = \frac{2}{3} \alpha \nu_{2t}$$

The friction coefficient is formulated as [36]:

$$\eta = \eta_1 + \frac{\eta_2 - \eta_1}{1 + \left(\frac{\left(I_o \right)}{\left[I_\upsilon + \alpha I_i^2 \right]^{1/2}} \right)}$$

where

$$I_\upsilon = \frac{2 \rho_2 \nu_2}{\phi_1 p_1} \left[\nabla \mathbf{u}_1 + \left(\nabla \mathbf{u}_1 \right)^T \right]$$

$$I_i = \frac{2d}{\sqrt{\phi_1\, p_1/\rho_1}}\left[\nabla \mathbf{u}_1 + \left(\nabla \mathbf{u}_1\right)^T\right]$$

Particle response time [37]:

$$\tau_p = \frac{\rho_1 d^2}{\rho_2 \nu_2}\frac{1}{a_E \phi_1^2 + b_E R_{e1}}$$

where

$$R_{e1} = \frac{\left|\mathbf{u}_2 - \mathbf{u}_1\right| d}{\nu_2}$$

Table 2
Model parameters

a	b	I_o	η_2	ϕ_1	ϕ_{1rcp}	K	C_μ
0.11	1	0.1	0.82	0.6	0.64	10^8 Pa	0.09
$C_{\varepsilon 1}$	$C_{\varepsilon 2}$	$C_{\varepsilon 3}$	α_k	α_ε	σ_c	a_E	b_E
1.44	1.92	1	1.5	1.3	1	1500	3.6

3. Results and Discussion

This study conducts simulations with the dual objectives of validating the model and exhibiting the model's capability in capturing the detailed mechanics of pipeline scouring and sedimentation. To achieve these objectives, we numerically replicate two experimental works of Mao [9] and Leckie *et al.,* [22], each pertaining to the phenomenon of scouring and sedimentation, respectively. The following subsections details the simulation conditions and the results obtained from both simulation scenarios.

3.1 Pipeline Scour Induced by Unidirectional Current

This section delves into the simulation of pipeline scour, which is conducted by replicating the experimental set-up of Mao [9]. The original experiment was conducted in a flume having dimensions of 23 m in length, 2 m in width, and 0.5 m in depth. Within this flume, a hydraulically smooth pipe of diameter $D = 0.05$ m was positioned above a 8 m-long and 0.1 m-thick section contained of uniform sediment particles. The sediment is characterized as coarse sand with the density of $\rho_s = 2600\left(\mathrm{kg/m^3}\right)$ and the median diameter of $d = 0.36$ mm. Initially, there was no gap between the pipe bottom and the surface of the sand bed, in which both were submerged in water with a constant depth of $h = 0.23$ m. The scour process was driven by unidirectional current from the inlet of the flume, approaching the pipe with an average velocity of $\overline{U} = 0.87$ m/s. According to Mao [8], this flow velocity corresponded to a Shields number of $\theta = 0.33$, which resulted in an intensive transport of sands across the flume in the live-bed regime.

The simulation set-up and parameters are directly drawn from the experiment, except the computational domain (shown in Figure 1) is made shorter with a total length of $20D$ for computational efficiency. The inlet, outlet, and top boundaries are defined as open boundaries, while the rigid bed and pipe surface are wall boundaries. The initial condition of the sand bed is assigned by static sands with concentration $\phi_1 = 0.55$, while the fluid region remains stationary. Notably, the present model accounts for the kinematics of both moving and static sand, including the process of bed consolidation. This interesting phenomenon is observed during the initial 0.5 s of the simulation.

Specifically, ϕ_1 exhibits vertical adjustment within a range of 0.55 to 0.56, extending from the bed surface to the bottom across the sand bed. At the inlet, positioned $6D$ upstream of the pipe, a logarithmic-law velocity profile with the average velocity of $\overline{U}$ is imposed. This velocity gradually ramps up linearly within $t \leq 4$ s to initiate the onset of scour smoothly. At this boundary, other fluid parameters and sediment parameters are set to have zero-gradient conditions. At the outlet, positioned $14D$ downstream of the pipe, all fluid and sediment parameters are set as zero-gradient. At the top boundary, a mixed Dirichlet–Neumann boundary condition is employed for the flow velocity, while the turbulent quantities follow the zero-gradient condition, and the pressure is defined as $p_f = 0$. On the rigid bed in between the inlet and the sand bed and at the pipe surface, a smooth wall function is implemented, and the pressure is maintained with a zero-gradient condition. The simulation runs for $t_s = 11$ s, corresponding to the earliest data of scour profile provided by the experiment [9]. This data will be used to validate the present model in simulating pipeline scour.

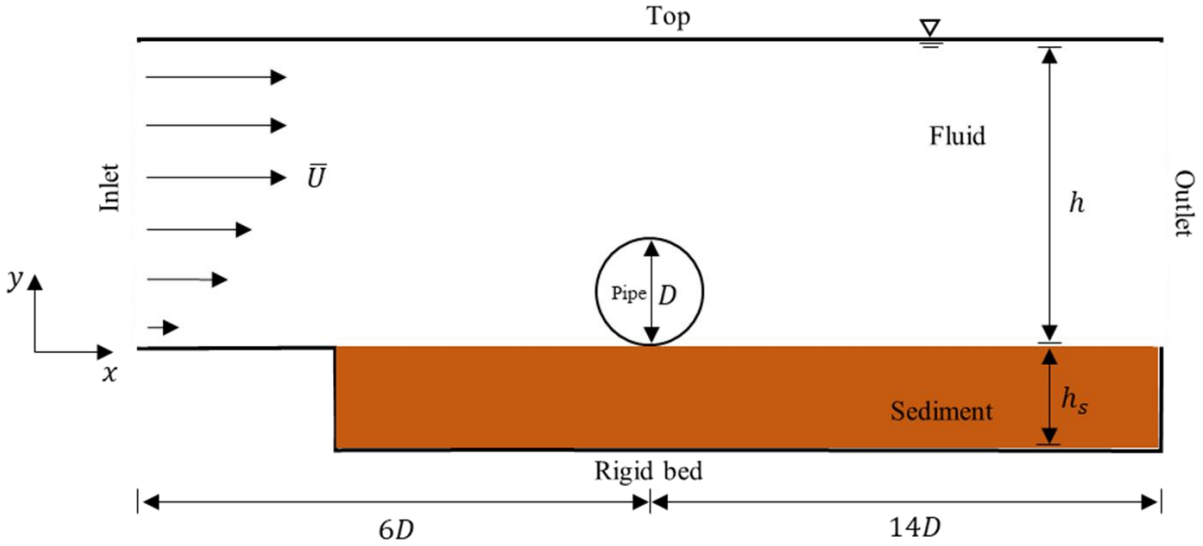

Fig. 1. Computational domain for the scour simulation case

The computational mesh is generated using the OpenFOAM utility named blockMesh. Further refinements, carried out by another utility named snappyHexMesh, are applied along the fluid-sediment interface and in the vicinity of the pipe structure. All cells in the mesh are rectangular in shape, with refined cells having dimension of $1.25\ \text{mm} \times 0.0625\ \text{mm}$ as shown in Figure 2. The selection of this cell size is based on the grid-independence test conducted during the validation of the present model for flow parameters around a pipe over a scoured bed. This validation was conducted by Tofany *et al.,* [33]. The simulation employing this grid size is executed in parallel using 16 threads of the ThinkStation-P358-Tower (AMD Ryzen™ 9 Pro 5945, CPU 3.0GHz, up to 4.7GHz with Turbo Boost, 12 cores, 24 threads, 64MB cache), resulting in a computational duration of approximately 6 hours.

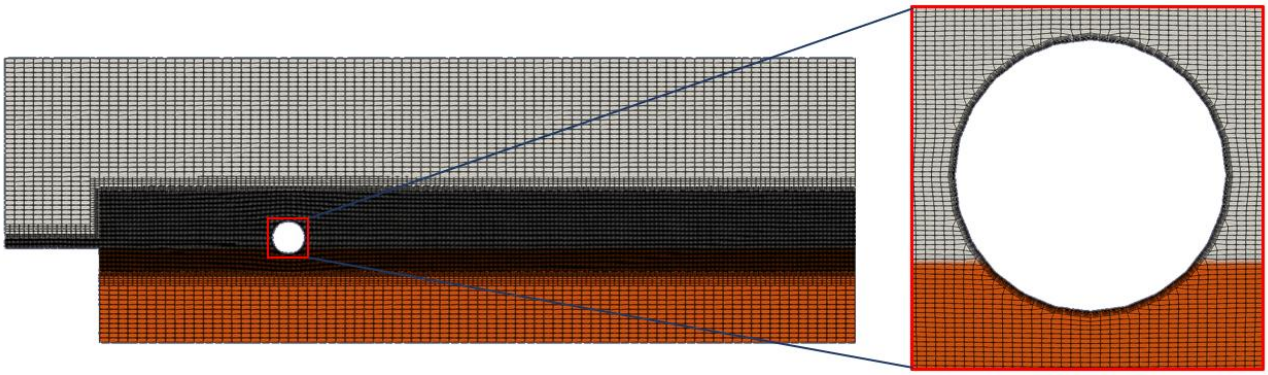

Fig. 2. Mesh diagram for the scour simulation case

The results of this simulation are displayed in Figure 3. Based on these results, important mechanisms (onset scouring, tunnel erosion, and lee wake erosion) in the scouring process of underwater pipes can be observed. Figures 3a and Figure 3b depict the mechanisms of onset scouring. Onset scouring represents the initial phase of erosion around the buried pipe [28, 34].

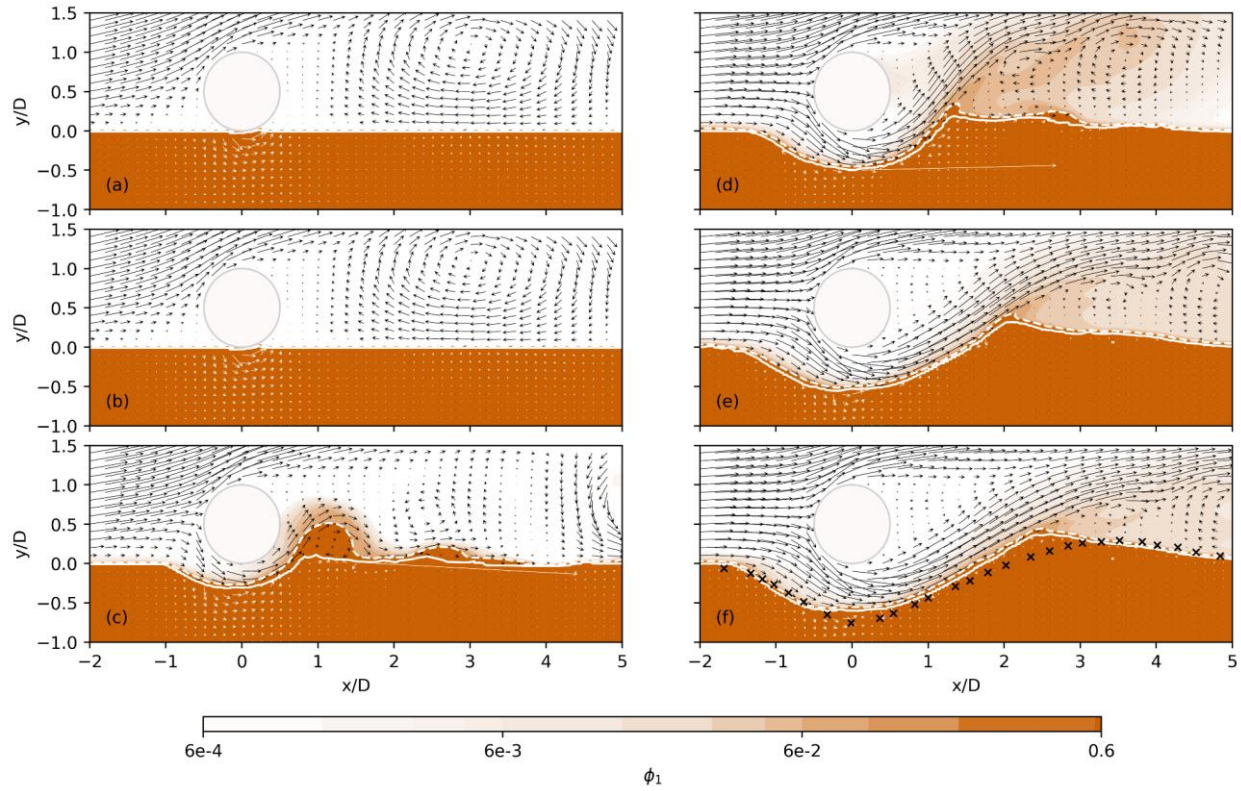

Fig. 3. Snapshots of sediment concentration contour (in logarithmic range) and fluid velocity vector fields during $3<t<11$ s: (a) $t=2$ s, (b) $t=3$ s, (c) $t=5$ s, (d) $t=7$ s, (e) $t=9$ s, (f) $t=11$ s. The white solid line presents the bed location that corresponds to $\phi_1=0.5$, while the white dashed line corresponds to $\phi_1=0.1$. The black cross points in the bottom panel (f) represent the measured profile [9]. The black/white arrows represent the fluid velocity fields above/within the bed

In these results, onset scouring occurs when $2<t<3$seconds. In Figures 3a and 3b, seepage flow in the sediment is evident, indicated by white arrows within the bed. This seepage flow occurs because the presence of the pipe causes pressure difference between the upstream and downstream parts of the pipe. The pressure difference is what causes the flow to seep into the sediment and

subsequently leads to seepage flow beneath the pipe. Over time, this seepage flow gradually causes a gentle movement of the bed leading to an initial gap opening beneath the pipe. Using the present model, Tofany and Wirahman [34] had revealed the detailed mechanism of the scour onset through a mechanism known as piping, which is mainly driven by the upstream-downstream pressure difference around the pipe.

In Figures 3c-d, the simulation results at $5 \le t \le 7$ s are shown. In these figures, an intense sediment transport that leads to a rapid erosion and thus trench formation is observed between the pipe and the bed. At the location $x/D \approx 1.2$, sediment suspensions with a height of approximately $y/D \approx 0.5$ is observed in Figure 3c. This occurs due to the immense amount of sediment beneath the pipe being transported by the accelerated flow in the gap towards downstream. Subsequently, this produces a high concentrated sediment-laden flow with concentration in the range of $0.3 \le \phi_1 \le 0.5$, spreading at the downstream within $0.8 \le x/D \le 3$. As shown in Figure 3d, these transported sediments are observed to accumulate at $1 \le x/D \le 3$ and a dune at the downstream appears to be forming. The simulation also shows a vortex stirring the sediment-laden flow at $x/D \approx 1.2$, which is believed contributing to the sediment deposition. This mechanism is typically referred to as tunnel erosion, which is mainly driven by the accelerated flow within the gap or known as the jet flow [7, 9].

Afterwards, the trench enlargement continues from $t = 7 - 11$ s (Figures 3e-f). The process is characterized by the trench deepening and widening with a slower rate where the downstream dune appears to grow larger and advance further. In Figure 3e, it can be seen that the dune reaches a peak height of $y/D \approx 0.4$ at $x/D \approx 2$, which moves to $x/D \approx 2.5$ at $t = 11$ s (Figure 3f). At this stage, the simulation shows that the transport of sediment is mainly in terms of bed-load transport, indicated by a thin layer of high-concentrated sediment $(0.3 \le \phi_1 \le 0.5)$ near the bed. Small suspended-load appears to concentrate at the vicinity of the dune peak, particularly within the area downstream of the dune that is being sheltered from the flow coming from the gap. This phase marks the beginning of lee wake erosion, characterized by a reduction in the intense sediment transport unlike what occurs during the tunnel erosion. Figure 3f shows the simulation results at $t = 11$ s where we compare this simulated profile with the results of Mao's experiment [9]. The black cross points in the lower panel (f) represent the profile measurements obtained from Mao's study in 1987. The white line represents the simulated profile. Based on Figure 3f, this simulated scouring process qualitatively agrees with the observations from the experimental study [9]. The morphology of the scour hole remains relatively stable between $t = 9$ s and $t = 11$ s, indicating that the lee-wake scour progresses at a significantly slower rate compared to tunnel scour. Despite its brief duration, tunnel erosion is the primary factor behind the significant enlargement of the scour trench beneath the pipe [23].

3.2 Pipeline Sedimentation Induced by Oscillatory Flow

In this case, the model application in simulating pipeline sedimentation process is presented. The sedimentation is driven by oscillatory flows generated by a regular sinusoidal fluid velocity time-series with the velocity amplitude u_m and period T as shown in Figure 4. The flow is generated through the body force terms in the momentum equations as presented in Table 1.

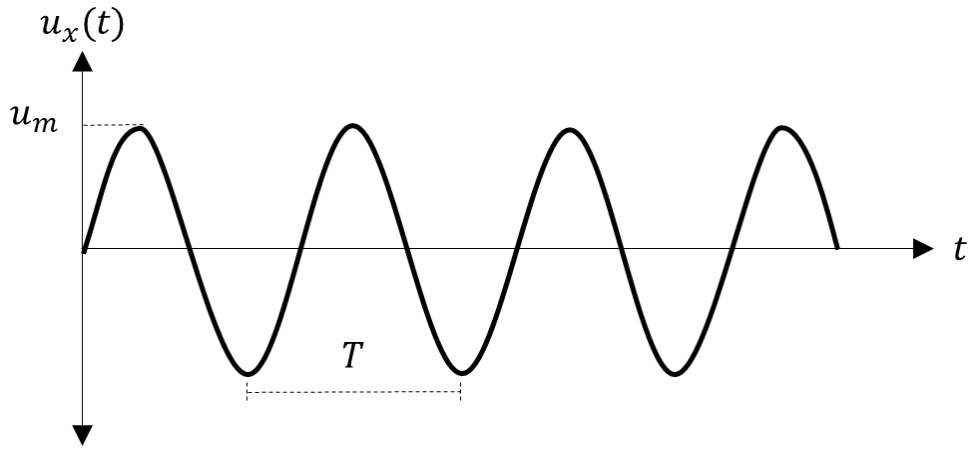

Fig. 4. Oscillatory flows

Two cases taken from the experiment of Leckie *et al.,* [22] are numerically simulated with simulation conditions are shown in Table 3. The two cases are different in terms of $KC = u_m T/D$ number and Shields number θ, in which Case B has higher KC and θ than Case A. Both cases are performed with the same sediment characteristics (silica sand with median diameter $d = 54$ mm and relative density $s = 2.75$, the pipe diameter of $D = 0.036$ m, and the water depth of $h = 0.2$ m. In the experiment Leckie *et al.,* [22], the initial burial depth of the pipeline and the flow conditions were selected to accurately mirror the real-world circumstances that were observed. The initial burial depth was uniformly set to $0.2D$ in both cases. This choice aimed to simulate the presumed depth at which the pipeline lies on the continental shelf, particularly where the most significant alterations in burial depth were noted.

Table 3
Simulation parameters for the sedimentation case

Case	$u_m\,(\mathrm{m/s})$	$T\,(\mathrm{s})$	KC	θ/θ_c
A	0.36	2.5	50	3.5
B	0.69	6.5	250	6

Figure 5 depicts the computational domain of this case. It comprises two main components: a sediment floor section having 8 m in length and 0.1 m in depth, which is submerged in a water section that is 2 m long and 0.2 m deep. The pipe is placed right in the middle of the domain above the sediment floor. This set up has the dimension that is half of the working section of the experiment [22] for computational efficiency. The left and right boundaries are defined as open boundaries, while the top, bottom, and pipe surface are defined as wall boundaries. The initial condition of the sand bed is assigned by static sands with concentration $\phi_1 = 0.6$, while the fluid region remains stationary. Same as in Section 3.1, the bed consolidates during the first 0.5 s of the simulation, in which the concentration varies vertically within a range of 0.6 to 0.61. All fluid and sediment parameters are set to have zero-gradient conditions at the open boundaries. A smooth wall function and the zero-gradient pressure are implemented at wall boundaries. The simulation runs for 100 s, which covers the time-scale of sedimentation observed in the experiment [22]. The blockMesh and snappyHexMesh utilities are used to generate the computational mesh with local refinements in the area along the upper part of the sediment floor. The refined area is around $2D$ in height, covering 15% of the upper-part of the sediment floor and 20% of the bottom part of the fluid section. All cells in the mesh are rectangular in shape, with refined cells having dimension of $2.5\ \mathrm{mm} \times 1.25\ \mathrm{mm}$ as

shown in Figure 6. Additionally, a body-conforming mesh is constructed around the pipe surface to accurately capture the boundary layer. The computations were conducted utilizing 16 processing threads from the ThinkStation-P358-Tower hardware (equipped with an AMD Ryzen™ 9 Pro 5945 CPU operating at 3.0GHz, capable of reaching 4.7GHz with Turbo Boost, featuring 12 cores, 24 threads, and a 64MB cache). These simulations required differing amounts of computational time, averaging approximately 24 hours, to simulate 150 seconds of physical time.

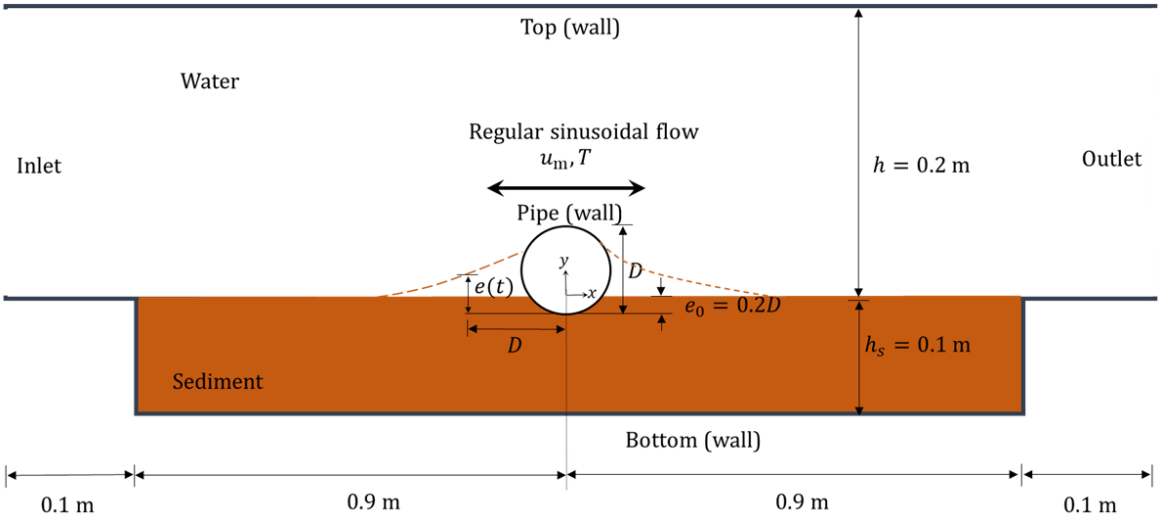

Fig. 5. Computational domain for the sedimentation case

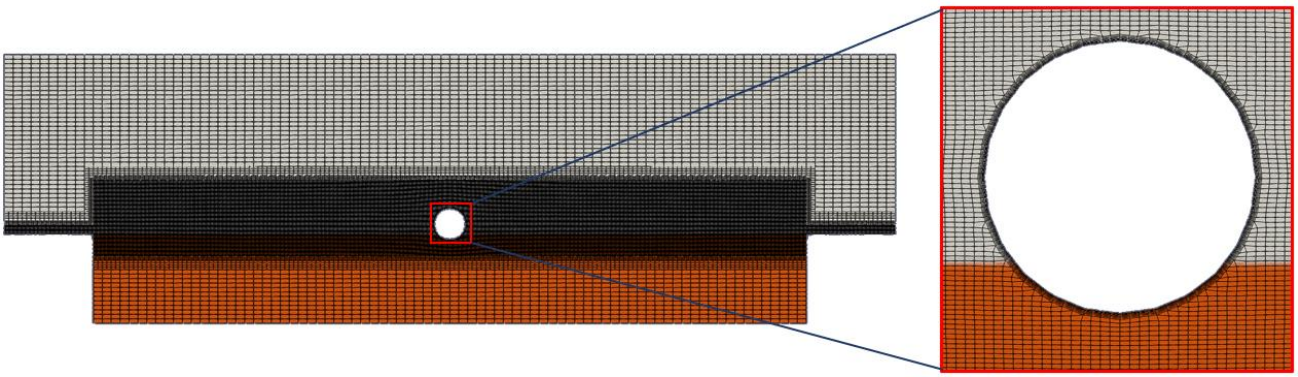

Fig. 6. Mesh diagram for the sedimentation case

Figure 7 illustrates the time series of the non-dimensional far-field flow velocity. In this figure, it is depicting that the oscillatory flow follows a sinusoidal pattern, symmetrical between the positive and negative directions. The positive direction represents the onshore flow (directed towards the right boundary), while the negative direction represents the offshore flow (directed towards the left boundary). To discuss the sediment concentration contour and flow velocity for each scenario, various points are selected, as depicted in Figure 7. Point (a) indicates a moment shortly after the onshore peak in the 2nd cycle, point (b) represents the offshore-onshore flow reversal in the 4th cycle, point (c) reflects a moment shortly after the offshore peak in the 8th cycle, and point (d) represents the onshore-offshore flow reversal in the 13th cycle.

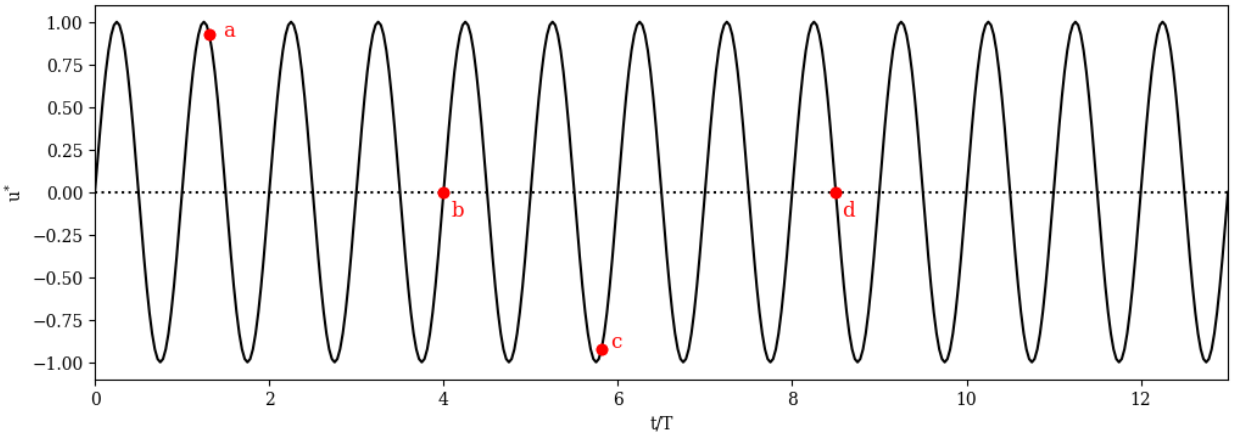

Fig. 7. Time series of the non-dimensional far-field flow velocity. Red dots represent the selected times to be discussed in Figure 8 and Figure 9

The simulation results of this sedimentation process are depicted in Figures 8 and 9. Figure 8 represents the simulation outcomes for parameter case A, while Figure 9 represents the simulation results for parameter case B. In case A, the simulation employs a sinusoidal oscillatory flow with a period of $T = 5$ s and a velocity amplitude of $0.36\,\mathrm{m/s}$. Meanwhile, in case B, a period of $T = 7$ s and a velocity amplitude of $0.51\,\mathrm{m/s}$ are used for the simulation. Figure 8a illustrates a moment after the onshore crest of the second cycle, occurring at $t = 6.5625$ s. At this moment, the fluid flow is predominantly directed towards the onshore, accompanied by the formation of a vortex at $x/D \approx 2.1$. The presence of this vortex disrupts the sediment bed in the onshore region, causing sediment to move toward the pipe direction. Consequently, this movement results in a slight sediment accumulation at $1 < x/D < 2$ and bed scouring at $x/D \approx 3$. When the simulation reaches $t = 20$ s, the flow approaches the offshore-onshore flow reversal, as depicted in Figure 8b. In this condition, not all of the main flow is directed towards the onshore direction; instead, some of the flow begins to reverse. At this moment, a higher sediment stack at $1 < x/D < 2$ and a deeper scoured-bed at $x/D \approx 3$ are observed compared to the $t = 6.5625$ s phase. They are resulted from sediment transported towards the pipe by the offshore-directed flow before the flow reversal.

Figure 8c represents the simulation at $t = 39.0625$ s, which corresponds to a moment after the offshore crest of the eighth cycle. In this condition, all the main flow is directed offshore, and a vortex form at $x/D \approx -2.2$. Through the same mechanism as during the onshore flow cycle (Figure 8a), this vortex disrupts bed stability in the offshore area, leading to sediment accumulation at $x/D \approx -1$. The oscillatory flow causes alternating disturbances in bed stability on both sides of the pipe, gradually resulting in sediment build-up around the pipe, as depicted in Figure 8d. Figure 8d portrays the sediment build-up condition close to equilibrium, occurring at $t = 62.5$ s. These results are also compared to the findings of Leckie's experiment [22]. The black cross points in Figure 8d represent the profile measurements obtained from Leckie's study, while the white line represents the simulated profile at $t = 62.5$ s. Based on these results, it can be observed that the simulation outcomes qualitatively agree with the observations from Leckie's experimental study [22].

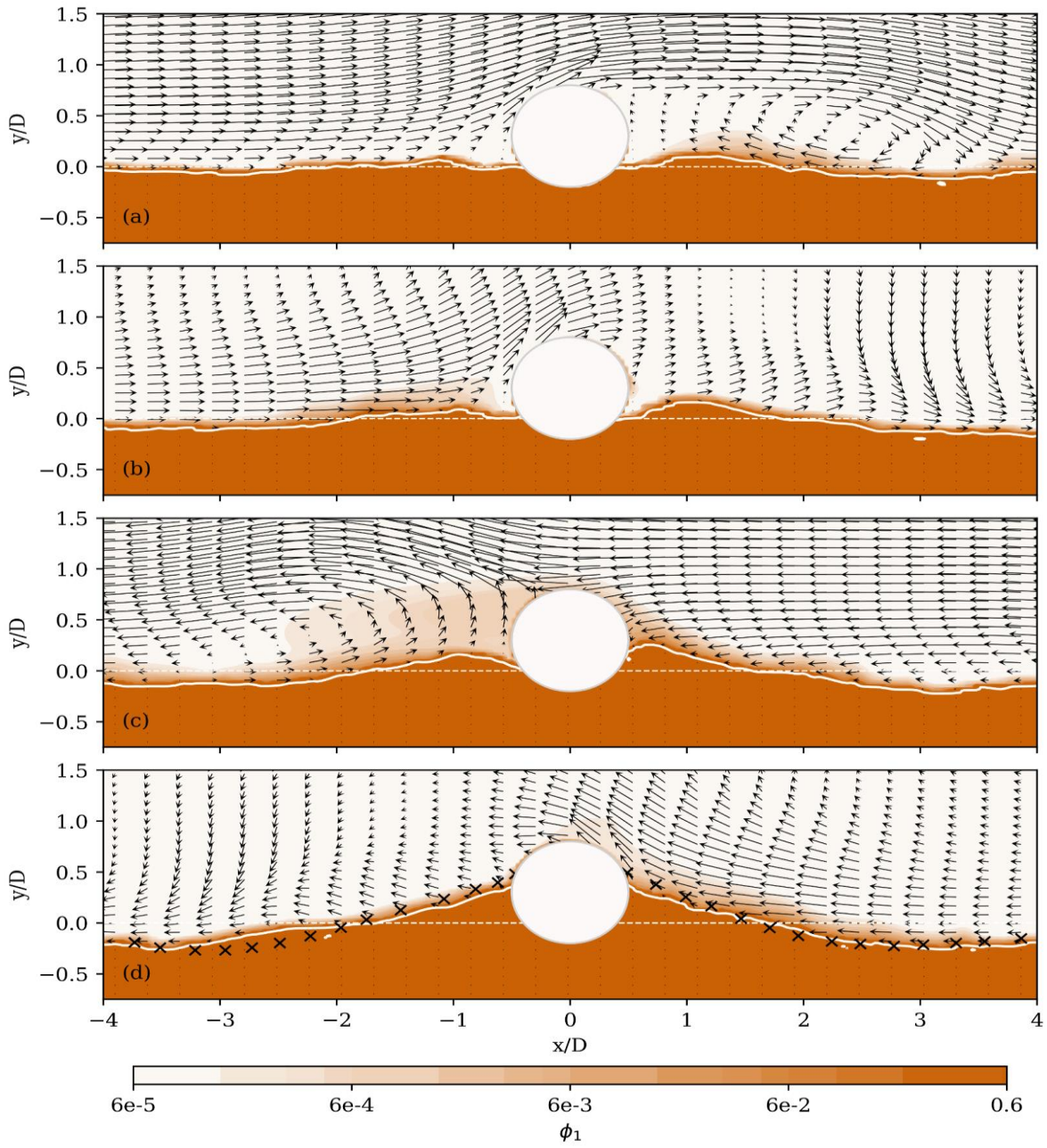

Fig. 8. Snapshot of sediment concentration contour (in logarithmic range) and flow velocity of Case A at (a) $t = 6.5625$ s (a moment after the onshore peak in the 2nd cycle), (b) $t = 20$ s (the offshore-onshore flow reversal in the 4th cycle), (c) $t = 39.0625$ s (a moment after the offshore peak in the 8th cycle), and (d) $t = 62.5$ s (the onshore-offshore flow reversal in the 13th cycle). The presented instants correspond to the red dots shown in Figure 7. The black-cross points in the bottom panel (d) represent the measured equilibrium bed profile [22]

Figure 9 depicts the simulation results for case B. In general, the simulation results for case B (Figure 9) are quite similar to those of case A (Figure 8). The fundamental difference between the two simulation results lies in the sedimentation process in case B being faster than that in case A. This is evident in Figure 9c, where at $t = 40.6875$ s, the simulation reaches a moment after the offshore crest of the eighth cycle. In this figure, it can also be seen that sediment accumulation has already started on both sides of the pipe. In contrast, in case A, sediment accumulation occurs on both sides during the onshore-offshore flow reversal in the 13th cycle with a duration of $t = 62.5$ s.

Figure 9d illustrates the simulation at $t = 59.5$ s. At this time, it is apparent that the sediment has reached close to equilibrium condition, burying the pipe with a height of approximately $y/D \approx 0.7$. This differs from the results in case A, where in case A, the sedimentation at this stage buries the pipe at a height of around $y/D \approx 0.5$. It appears that the difference in the burial rate of the pipe and the height of sediment burial around the pipe is strongly influenced by the KC and Shield numbers assigned in the simulation. It is observed that larger KC and Shield numbers (Case B) lead to a faster burial time and a higher burial height around the pipe. In Figure 9d, the measured bed profile at close to equilibrium condition is overlayed to validate the model. It can be seen from the comparison that the present model is capable of closely replicating the measured profile, demonstrating its predictive capability.

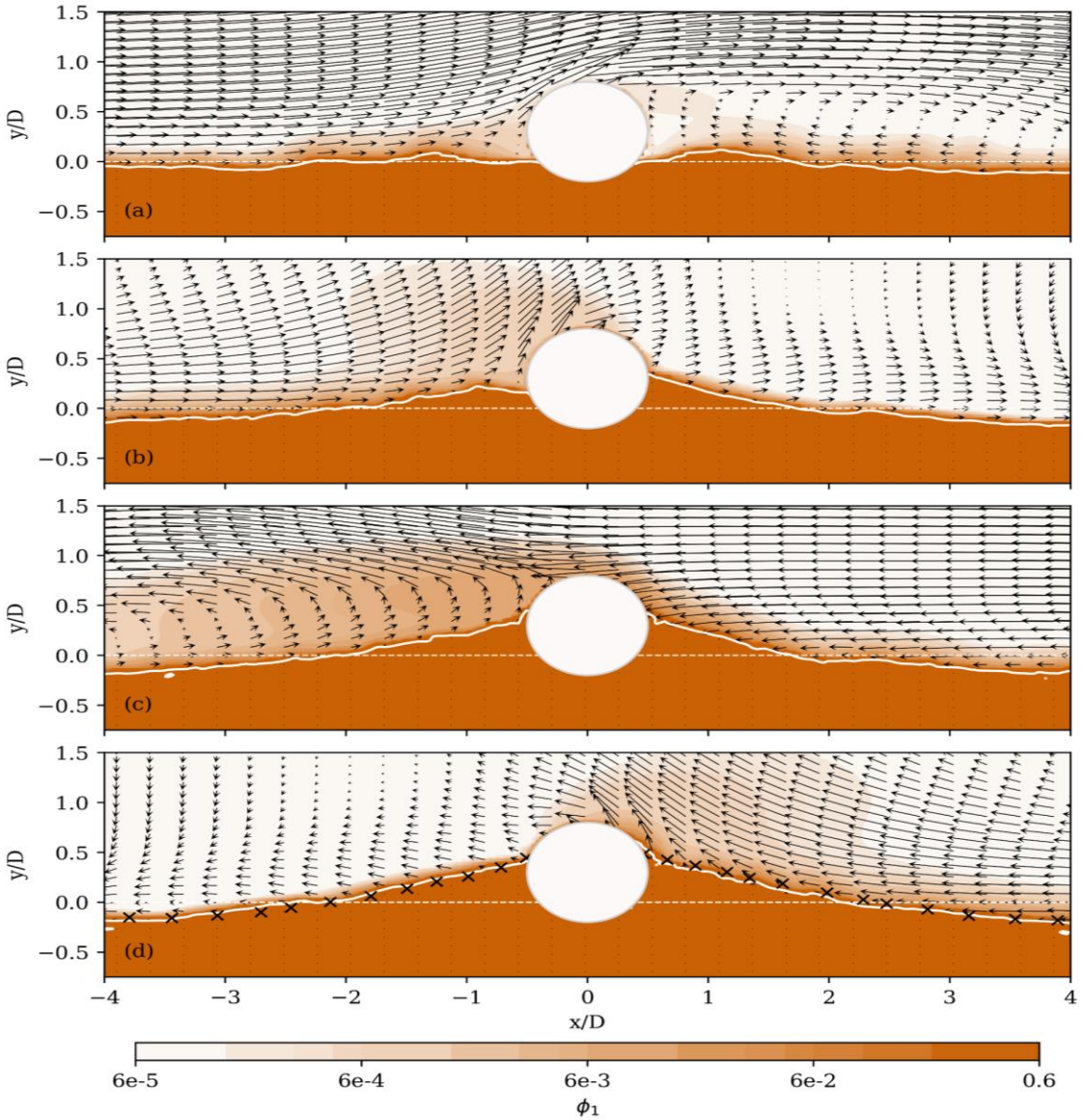

Fig. 9. Snapshots of sediment concentration contour (in logarithmic range) and flow velocity of Case B at (a) $t = 9.1875$ s (a moment after the onshore peak in the 2nd cycle), (b) $t = 28$ s (the offshore-onshore flow reversal in the 4th cycle), (c) $t = 40.6875$ s (a moment after the offshore peak in the 8th cycle), and (d) $t = 59.5$ s (the onshore-offshore flow reversal in the 13th cycle). The presented instants correspond to the red dots shown in Figure 7. The black-cross points in the bottom panel (d) represent the measured equilibrium bed profile [22]

4. Conclusions

In this paper, a two-phase CFD model using the Eulerian-Eulerian approach is employed to simulate the early stages of scour beneath a submarine pipeline, encompassing both the onset and tunnel erosion as well as the burial of the pipeline due to sediment accumulation under oscillatory flow conditions, considering different KC numbers and shield stress levels. The present two-phase model integrates the interaction between fluid and sediment dynamics, encompassing closure models and constitutive relationships for interactions between fluid and particles, as well as particles amongst themselves. As a result, the model is capable of calculating sediment transport without relying on conventional assumptions regarding bed-load and suspended-load layers. The simulation results demonstrate the model's effectiveness in reproducing the driving mechanism responsible for the onset, specifically the seepage flow that is important for piping, and the generation of jet-like flow beneath the pipe as the driving mechanism for tunnel erosion. In addition, this model can also capture the complex interaction between the vortices generated at the lee-wake with the sediment particles, which determine the sedimentation process around the pipe and the resulting local burial depth in different oscillatory flow conditions. More importantly, the simulated results show consistent results with the experimental observations in both scour and sedimentation cases. These advantages and successful validations enhance the utility of the model in elucidating the fundamental mechanisms governing the initial phases of scour and sedimentation around the pipeline. The implementation of a multiphase-CFD model enhances the predictive capabilities of engineers. It enables them to anticipate and mitigate the effects of scour and sedimentation on submerged pipelines with greater precision. The research provides a comprehensive understanding of the scour and sedimentation processes around submerged pipelines. This knowledge is essential for engineers involved in the design, maintenance, and optimization of underwater structures, including pipelines.

Acknowledgement
This research was funded by Fundamental Research (PRF) of the Ministry of Education, Culture, Research, and Technology (grant number 148/E5/PG.02.00.PL/2023), the Educational Fund Management Institution (LPDP) of the Ministry of Finance the Republic of Indonesia (RIIM Grant B-1736/II.7.5/FR/11/2022) and National Research and Innovation Agency of Indonesia (BRIN) through RPOREI-AIBDTK2023 and its postdoctoral program. The author would like to thank the Dean of the Faculty of Fishery and Marine Science and the Directorate of Research and Community Service, Universitas Padjadjaran for support this work.

References

[1] Wang, Guotao, Qianwei Cheng, Wei Zhao, Qi Liao, and Haoran Zhang. "Review on the transport capacity management of oil and gas pipeline network: Challenges and opportunities of future pipeline transport." *Energy Strategy Reviews* 43 (2022): 100933. https://doi.org/10.1016/j.esr.2022.100933

[2] Vosoughi, Hassan, and Hooman Hajikandi. "Scour around submarine pipes due to high-amplitude transient waves." *Water Science and Engineering* 13, no. 2 (2020): 154-161. https://doi.org/10.1016/j.wse.2020.06.003

[3] Draper, Scott, John M. Harris, Liang Cheng, and David J. White. "Seabed processes: Sediment transport, scour, and sedimentation." *Encyclopedia of Maritime and Offshore Engineering* (2017): 1-11. https://doi.org/10.1002/9781118476406.emoe539

[4] Aryawan, Wasis Dwi, I. Ketut Aria Pria Utama, and Yuda Apri Hermawan. "CFD Analysis into the Resistance Characteristics of Remotely Operated Vehicles when Submerges Under Water and Sails on the Surface." *CFD Letters* 15, no. 8 (2023): 166-178. https://doi.org/10.37934/cfdl.15.8.166178

[5] Najafzadeh, Mohammad, and Giuseppe Oliveto. "Scour propagation rates around offshore pipelines exposed to currents by applying data-driven models." *Water* 14, no. 3 (2022): 493. https://doi.org/10.3390/w14030493

[6] Silvia, Cut Suciatina, Muhammad Ikhsan, and Azwanda Azwanda. "The Effect of Bridge Piers on Local Scouring at Alue Buloh Bridge Nagan Raya Regency." In *Journal of the Civil Engineering Forum*, vol. 7, no. 1, pp. 37-46. https://doi.org/10.22146/jcef.57719

[7] Chiew, Yee-Meng. "Mechanics of local scour around submarine pipelines." *Journal of Hydraulic Engineering* 116, no. 4 (1990): 515-529. https://doi.org/10.1061/(ASCE)0733-9429(1990)116:4(515)

[8] Sumer, B. Mutlu, Christoffer Truelsen, T. Sichmann, and Jørgen Fredsøe. "Onset of scour below pipelines and self-burial." *Coastal engineering* 42, no. 4 (2001): 313-335. https://doi.org/10.1016/S0378-3839(00)00066-1

[9] Mao, Ye. "The interaction between a pipeline and an erodible bed." *Series Paper Technical University of Denmark* 39 (1987).

[10] Sumer, B. Mutiu, and Jørgen Fredsøe. "Scour below pipelines in waves." *Journal of waterway, port, coastal, and ocean engineering* 116, no. 3 (1990): 307-323. https://doi.org/10.1061/(ASCE)0733-950X(1990)116:3(307)

[11] Sumer, B. Mutlu. *The mechanics of scour in the marine environment*. World Scientific, 2002. https://doi.org/10.1142/4942

[12] Tom, Joe G., Simon HF Leckie, David J. White, and Scott Draper. "Drained breakout resistance of a pipeline on a mobile seabed." In *International Conference on Offshore Mechanics and Arctic Engineering*, vol. 56529, p. V05BT04A057. American Society of Mechanical Engineers, 2015. https://doi.org/10.1115/OMAE2015-41206

[13] Bransby, Fraser, Antonio Borges Rodriguez, Hongjie Zhou, Joe Tom, Han Eng Low, and David White. "Sediment mobility effects on seabed resistance for unburied pipelines." In *Offshore Technology Conference*, p. D031S032R006. OTC, 2014. https://doi.org/10.4043/25287-MS

[14] Ho, Michael, Sami El-Borgi, Devendra Patil, and Gangbing Song. "Inspection and monitoring systems subsea pipelines: A review paper." *Structural Health Monitoring* 19, no. 2 (2020): 606-645. https://doi.org/10.1177/1475921719837718

[15] Chiew, Yee-Meng. "Prediction of maximum scour depth at submarine pipelines." *Journal of Hydraulic Engineering* 117, no. 4 (1991): 452-466. https://doi.org/10.1061/(ASCE)0733-9429(1991)117:4(452)

[16] Dey, Subhasish, and Navneet P. Singh. "Clear-water scour below underwater pipelines under steady flow." *Journal of hydraulic engineering* 134, no. 5 (2008): 588-600. https://doi.org/10.1061/(ASCE)0733-9429(2008)134:5(588)

[17] Penna, Nadia, Francesco Coscarella, and Roberto Gaudio. "Turbulent flow field around horizontal cylinders with scour hole." *Water* 12, no. 1 (2020): 143. https://doi.org/10.3390/w12010143

[18] Wu, Yushi, and Yee-Meng Chiew. "Mechanics of three-dimensional pipeline scour in unidirectional steady current." *Journal of Pipeline Systems Engineering and Practice* 4, no. 1 (2013): 3-10. https://doi.org/10.1061/(ASCE)PS.1949-1204.0000118

[19] Wu, Yushi, and Yee-Meng Chiew. "Three-dimensional scour at submarine pipelines." *Journal of Hydraulic Engineering* 138, no. 9 (2012): 788-795. https://doi.org/10.1061/(ASCE)HY.1943-7900.0000583

[20] Fuhrman, David R., Cüneyt Baykal, B. Mutlu Sumer, Niels G. Jacobsen, and Jørgen Fredsøe. "Numerical simulation of wave-induced scour and backfilling processes beneath submarine pipelines." *Coastal engineering* 94 (2014): 10-22. https://doi.org/10.1016/j.coastaleng.2014.08.009

[21] Larsen, Bjarke Eltard, David R. Fuhrman, and B. Mutlu Sumer. "Simulation of wave-plus-current scour beneath submarine pipelines." *Journal of Waterway, Port, Coastal, and Ocean Engineering* 142, no. 5 (2016): 04016003. https://doi.org/10.1061/(ASCE)WW.1943-5460.0000346

[22] Leckie, Simon HF, Henning Mohr, Scott Draper, Dianne L. McLean, David J. White, and Liang Cheng. "Sedimentation-induced burial of subsea pipelines: Observations from field data and laboratory experiments." *Coastal Engineering* 114 (2016): 137-158. https://doi.org/10.1016/j.coastaleng.2016.04.017

[23] Liang, Dongfang, Liang Cheng, and Fangjun Li. "Numerical modeling of flow and scour below a pipeline in currents: Part II. Scour simulation." *Coastal engineering* 52, no. 1 (2005): 43-62. https://doi.org/10.1016/j.coastaleng.2004.09.001

[24] Liu, Ming-ming, Lin Lu, Bin Teng, Ming Zhao, and Guo-qiang Tang. "Numerical modeling of local scour and forces for submarine pipeline under surface waves." *Coastal Engineering* 116 (2016): 275-288. https://doi.org/10.1016/j.coastaleng.2016.05.003

[25] Zhao, Ming, Shailesh Vaidya, Qin Zhang, and Liang Cheng. "Local scour around two pipelines in tandem in steady current." *Coastal Engineering* 98 (2015): 1-15. https://doi.org/10.1016/j.coastaleng.2015.01.001

[26] Zhao, Enjin, Bing Shi, Ke Qu, Wenbin Dong, and Jing Zhang. "Experimental and numerical investigation of local scour around submarine piggyback pipeline under steady current." *Journal of Ocean University of China* 17 (2018): 244-256. https://doi.org/10.1007/s11802-018-3290-7

[27] Zhao, Enjin, Ke Qu, Lin Mu, Simon Kraatz, and Bing Shi. "Numerical study on the hydrodynamic characteristics of submarine pipelines under the impact of real-world tsunami-like waves." *Water* 11, no. 2 (2019): 221. https://doi.org/10.3390/w11020221

[28] Liang, Dongfang, Tiejian Li, and Yang Xiao. "Simulation of scour around a vibrating pipe in steady currents." *Journal of Hydraulic Engineering* 142, no. 2 (2016): 04015049. https://doi.org/10.1061/(ASCE)HY.1943-7900.0001084
[29] Baharin, Nur Marissa Kamarul, Mohd Azan Mohammed Sapardi, Nur Nadhirah Ab Razak, Ahmad Hussein Abdul Hamid, and Syed Noh Syed Abu Bakar. "Study on Magnetohydrodynamic Flow Past Two Circular Cylinders in Staggered Arrangement." *CFD Letters* 13, no. 11 (2021): 65-77. https://doi.org/10.37934/cfdl.13.11.6577
[30] Tung, Pham Duy, Tomoaki Watanabe, and Koji Nagata. "Large-eddy simulation of a flow generated by a piston-driven synthetic jet actuator." *CFD Letters* 15, no. 8 (2023): 1-18. https://doi.org/10.37934/cfdl.15.8.118
[31] Hassim, Muhammad Ridhwaan, Mohd Azan Mohammed Sapardi, Nur Marissa Kamarul Baharin, Syed Noh Syed Abu Bakar, Muhammad Abdullah, and Khairul Affendy Mohd Nor. "CFD Modelling of Wake-Induced Vibration At Low Reynolds Number." *CFD Letters* 13, no. 11 (2021): 53-64. https://doi.org/10.37934/cfdl.13.11.5364
[32] Lee, Cheng-Hsien. "Multi-phase flow modeling of submarine landslides: Transformation from hyperconcentrated flows into turbidity currents." *Advances in Water Resources* 131 (2019): 103383. https://doi.org/10.1016/j.advwatres.2019.103383
[33] Tofany, Novan, David Eka Putra, and Arnida L. Latifah. "Current-induced scouring around a submarine pipeline using a multi-phase flow model with different inter-phase drag models." *Ocean Engineering* 286 (2023): 115691. https://doi.org/10.1016/j.oceaneng.2023.115691
[34] Tofany, Novan, and Taufiq Wirahman. "Numerical simulation of early stages of scour around a submarine pipeline using a two-phase flow model." *Ocean Engineering* 264 (2022): 112503. https://doi.org/10.1016/j.oceaneng.2022.112503
[35] Lee, Cheng-Hsien, Ying Min Low, and Yee-Meng Chiew. "Multi-dimensional rheology-based two-phase model for sediment transport and applications to sheet flow and pipeline scour." *Physics of Fluids* 28, no. 5 (2016). https://doi.org/10.1063/1.4948987
[36] Trulsson, Martin, Bruno Andreotti, and Philippe Claudin. "Transition from the viscous to inertial regime in dense suspensions." *Physical review letters* 109, no. 11 (2012): 118305. https://doi.org/10.1103/PhysRevLett.109.118305
[37] Engelund, Frank, and Jørgen Fredsøe. "A sediment transport model for straight alluvial channels." *Hydrology Research* 7, no. 5 (1976): 293-306. https://doi.org/10.2166/nh.1976.0019